Journal of Biomechanics 95 (2019) 109315

Contents lists available at ScienceDirect

Journal of Biomechanics

journal homepage: www.elsevier.com/locate/jbiomech
www.JBiomech.com

Predicted threshold against forward and backward loss of balance for perturbed walking

Hosein Bahari [a], Albert H. Vette [a,c], Jacqueline S. Hebert [b,c], Hossein Rouhani [a,c,*]

[a] Department of Mechanical Engineering, University of Alberta, Donadeo Innovation Centre for Engineering, Edmonton, Alberta T6G 1H9, Canada
[b] Department of Medicine, University of Alberta, Katz Group Centre, Edmonton, Alberta T6G 2E1, Canada
[c] Glenrose Rehabilitation Hospital, Alberta Health Services, 10230 – 111 Avenue NW, Edmonton, Alberta T5G 0B7, Canada

ARTICLE INFO

Article history:
Accepted 11 August 2019

Keywords:
Dynamic optimization
Fall prevention
Forward dynamics
Musculoskeletal modeling
Walking stability

ABSTRACT

The biomechanical mechanisms of loss of balance have been studied before for slip condition but have not been investigated for arbitrary perturbation profiles under non-slip conditions in sagittal plane. This study aimed to determine the thresholds of center of mass (COM) velocity and position relative to the base of support (BOS) that predict forward and backward loss of balance during walking with a range of BOS perturbations. Perturbations were modeled as sinusoidal BOS motions in the vertical or anterior-posterior direction or as sagittal rotation. The human body was modeled using a seven-link model. Forward dynamics alongside with dynamic optimization were used to find the thresholds of initial COM velocity for each initial COM position that would predict forward or backward loss of balance. The effects of perturbation frequency and amplitude on these thresholds were modeled based on the simulation data. Experimental data were collected from 15 able-bodied individuals and three individuals with disability during perturbed walking. The simulation results showed similarity with the stability region reported for slip and non-slip conditions. The feasible stability region shrank when the perturbation frequency and amplitude increased, especially for larger initial COM velocities. 89.5% (70.9%) and 82.4% (68.2%) of the measured COM position and velocity combinations during low (high) perturbations were located inside the simulated limits of the stability region, for able-bodied and disabled individuals, respectively. The simulation results demonstrated the effects of different perturbation levels on the stability region. The obtained stability region can be used for developing rehabilitative programs in interactive environments.

1. Introduction

At least 10–20% of falls lead to injuries that require medical attention (Stevens and Sogolow, 2005). Understanding mechanisms of falling can help prevent consequences of falls by developing preventive strategies that can help individuals to maintain balance. A majority of falls occur during locomotion, such as gait (Robinovitch et al., 2013). Human gait stability and its correlation with the variability of gait parameters have long been studied using various mathematical tools (Anderson and Pandy, 2001; Bruijn et al., 2013; Hausdorff et al., 2001; Wolf et al., 1985). However, the extent to which these mathematical measures are reliable for perturbed walking circumstances is a matter of debate (Bruijn et al., 2013; Madehkhaksar et al., 2018).

Biomechanical mechanisms of walking stability can be characterized by the state of center of mass (COM) motion (i.e., its position and velocity) with respect to its base of support (BOS) (Hof et al., 2005; Pai et al., 1998; Yang et al., 2009). Concepts such as the extrapolated COM (Hof, 2008) and feasible stability region (FSR) (Pai et al., 2000; Yang et al., 2009) were introduced to identify possible combinations of COM motion states for which an individual can maintain balance during a gait cycle. In general, if the COM motion states during walking are within the FSR, loss of balance is not likely to occur. If these states lie below the lower boundary of FSR or above the higher boundary of FSR, backward or forward loss of balance, respectively, is most probable to happen (Pai, 2003).

Previously, dynamics of gait and its stability in the sagittal plane were studied using one-link (Kuo et al., 2005), two-link (Goswami et al., 2006), five-link (Hurmuzlu, 1993), and twelve-link models (Delp et al., 2007). Also, various models were utilized to find the FSR for walking and standing in the sagittal plane and their results varied as a function of the number of links (Yang et al., 2008); nevertheless, general agreement with the

* Corresponding author at: Department of Mechanical Engineering, University of Alberta, 10-368 Donadeo Innovation Centre for Engineering, 9211 – 116 Street NW, Edmonton, Alberta T6G 1H9, Canada.
E-mail address: hrouhani@ualberta.ca (H. Rouhani).

https://doi.org/10.1016/j.jbiomech.2019.109315
0021-9290/

experimental data was found. In addition, FSR during gait followed by a slip was studied using a seven-segment model and a complex optimization routine that incorporated the physiological, geometrical, and biomechanical limits during walking (Yang et al., 2008). Yet, only 5% of falls among the elderly residing in long-term care facilities occur due to slipping (Robinovitch et al., 2013) and the FSR for other walking perturbation conditions is unknown.

Rehabilitative training using virtual reality interactive environments, such as Computer-Assisted Rehabilitation ENvironment (CAREN), has shown potential in improving walking balance and reducing the incidence of falling (McAndrew et al., 2011). Such setups are able to duplicate challenging walking conditions during daily life based on the application of oscillatory motions to a platform-mounted treadmill on which the user walks. A prerequisite to the development of efficient rehabilitative training is to characterize the FSR due to each perturbation condition and train the users to maintain their COM motion states inside the FSR in the presence of these walking perturbations. It is challenging to characterize FSR for every type of walking perturbation, separately, and tune the training program accordingly, since the types of walking perturbation that may cause falling are numerous. To obtain FSR during a wide range of walking perturbations in an interactive rehabilitative setup (e.g., CAREN), we propose to model the applied perturbations using a combination of sinusoidal motions of the BOS in the three anatomical planes. We hypothesized that obtaining FSR as a function of amplitude and frequency of these sinusoidal motions of the BOS can characterize the FSR for complex BOS motions. In this study, we only focused on BOS perturbations in the sagittal plane (vertical direction, horizontal direction and the rotation in the sagittal plane), and we suggested characterizing the FSR for other types of BOS perturbation in the future studies. As such, any forward or backward loss of balance due to BOS perturbation in the sagittal plane can be characterized based on these three BOS motion modalities.

Our primary objective was to find the effect of external perturbations, modeled using sinusoidal BOS motion, on FSR and, thus, to offer a framework to evaluate the dynamic stability of perturbed walking in the sagittal plane due to complex BOS motions. Our secondary objective was to validate the obtained FSR using experimental data from perturbed walking in an interactive setup, i.e., CAREN.

2. Methods

2.1. Modeling of loss of balance during perturbed walking

A seven-segment bipedal model of the human body in the sagittal plane was used based on a previously developed model by Yang et al. (2008) (Fig. 1.a). The details of this model are presented in the Supplementary material. We implemented this model in Simulink (Mathworks, USA). The initial COM positions were systematically chosen to be $[-2, -1.75, -1.5, -1.25, -1, -0.75, -0.5, -0.25, 0] \times$ *foot length*, with respect to the toes (posterior edge of the foot), where 0 and -1 indicate the COM being positioned right above the toe and heel, respectively. Body segments' configurations for each chosen initial COM position were adopted from our experimental data.

At each initial COM position, we used a Genetic Algorithm (GA) optimization to obtain the feasible maximum and minimum COM velocities that would result in COM motion ending within the BOS. These maximum and minimum COM velocities determined the thresholds against backward and forward loss of balance. Inputs to the model included the initial angle and angular velocity of each joint (θ, $\dot{\theta}$), along with their muscle excitation history, modeled using 76 control nodes (Fig. 2). Two separate optimization cost functions (CF) were used to find the maximum and minimum feasible initial velocities to prevent forward and backward loss of balance. In order to enable characterizing the stability of perturbed walking and modeling a smooth and natural progression of swing phase of gait, we revised the cost function introduced by Yang et al. (2008):

$$\begin{aligned} CF_{backward} = {} & w_1\, \dot{x}_{COM}^{initial} + w_2 \left|\dot{x}_{COM}^{final}\right| + w_3 \int_{t_i}^{t_f} e\left(F_y(t)\right)dt \\ & + w_4 \int_{t_i}^{t_f} e(\theta(\mathrm{t}))dt + w_5 \int_{t_i}^{t_f} e\left(\dot{\theta}(\mathrm{t})\right)dt \\ & + w_6 \int_{t_i}^{t_f} \min\left(y_{l,toe}(t), y_{l,heel}(t)\right)dt + w_7 e\left(x_{COM}^{final} - x_{r,heel}^{final}\right) \\ & + w_8 \int_{t_i}^{t_f} \tau(t)^2 dt + w_9 x_{l,heel}^{final} - x_{r,toe}^{final} \\ & + w_{10} \left|y_{HAT\ COM}^{initial} - y_{HAT\ COM}^{final}\right| \\ & + w_{11} \int_{t_i}^{t_f} e\left(y_{l,heel} - y_{r,heel}\right)dt + w_{12} \sum_{i=1}^{6} \int_{t_i}^{t_f} SD(\theta_{\mathrm{i}})dt \end{aligned} \quad (1)$$

In Eq. (1), integrals were taken over the simulation time to ensure that no physiological constraint is violated during the simulation. Subscripts r and l indicate right and left foot, and t_i, t_f indicate the initial and final time instance of the simulation, respectively. The $e(x(t))$ and $\lfloor x(t) \rfloor$ functions and the rationale for including the first to eighth terms in the cost function has been discussed in (Yang et al., 2008). However, we added terms 9, 10, 11, and 12 to the previously developed cost function. The ninth term ensures the left foot is placed in front of the right foot at the end of simulation and a complete swing phase is performed. The tenth term ensures the HAT segment has physiologically meaningful motions. The eleventh term guarantees the left heel is in contact with the ground at the end of simulation. Finally, the twelfth term ensures each segment's angle changes smoothly and does not illustrate rapid movements (SD: standard deviation). Adding these terms is important for perturbation analyses where relative motion of body segments is important compared to the unperturbed case where the support surface is motionless. These terms particularly, assured physiologically meaningful sway of the HAT segment and a smooth leg swing during perturbed gait.

A similar cost function was used to find the maximum initial velocity:

$$\begin{aligned} CF_{forward} = {} & w_1\, /\dot{x}_{COM}^{initial} + w_2 \left|\dot{x}_{COM}^{final}\right| + w_3 \int_{t_i}^{t_f} e\left(F_y(t)\right)dt \\ & + w_4 \int_{t_i}^{t_f} e(\theta(\mathrm{t}))dt + w_5 \int_{t_i}^{t_f} e\left(\dot{\theta}(\mathrm{t})\right)dt \\ & + w_6 \int_{t_i}^{t_f} \min\left(y_{l,toe}(t), y_{l,heel}(t)\right)dt + w_7 e\left(x_{COM}^{final} - x_{r,toe}^{final}\right) \\ & + w_8 \int_{t_i}^{t_f} \tau(t)^2 dt + w_9 x_{l,heel}^{final} - x_{r,toe}^{final} + w_{10} \left|y_{HAT\ COM}^{initial} - y_{HAT\ COM}^{final}\right| \\ & + w_{11} \int_{t_i}^{t_f} e\left(y_{l,heel} - y_{r,heel}\right)dt + w_{12} \sum_{i=1}^{6} \int_{t_i}^{t_f} SD(\theta_{\mathrm{i}})dt \end{aligned} \quad (2)$$

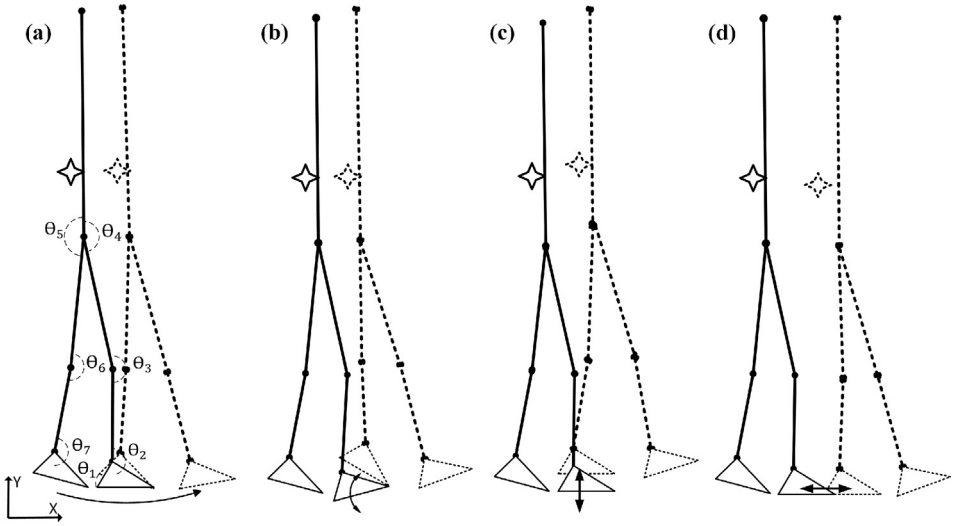

Fig. 1. (a) Schematic of the bipedal human model in the sagittal plane. The model parameters were defined by a group of joint angles (θ_1, θ_2, …, θ_7). The planar motion of the right foot was reduced to a revolute motion around the anterior edge of the foot (right toe) to reconstruct a non-slip situation. The physiological range of motion was used as a constraint for each joint's motion. The model was built based on an 80 kg weighted and 1.8 m tall person's anthropometric data adapted from literature (Winter, 2005). (b), (c), and (d) show the base of support (BOS) perturbation as a rotation in the sagittal plane, a vertical displacement, and a horizontal displacement, respectively.

The change in the first and seventh term was made to obtain the maximum initial velocity and to end the swing phase with a COM position behind the front end of BOS (right toe), respectively. A trial and error approach was used to determine the optimal weight of each term in both cost functions (w_i). In all simulations, the right foot was assumed to be fixed to the BOS, and the COM motion states were calculated with respect to the BOS.

Notably, the obtained FSRs were pertaining to the toe-off instance of the left foot. As such, the backward loss of balance was defined as a necessity to take a step backward to maintain balance. Also, the forward loss of balance was defined as the inability to maintain balance by terminating gait where the right foot is located and a necessity to take at least one step forward by the left foot. Forward loss of balance continuously occurs during walking and its limit is relevant only to characterize the stability of gait termination.

2.2. FSR limits as a function of BOS perturbation in the sagittal plane

The three BOS motion modalities were modelded as sinusoidals: translational in the vertical direction and in the horizontal (anterior-posterior) direction, and rotational in the sagittal plane (Fig. 1.b to 1.d). The amplitude of these sinusoidals was assumed to be 5 cm, 10 cm, and 15 cm for vertical and horizontal displacements and 1.5°, 5°, and 10° for sagittal rotations. Their frequency was assumed to be 1 Hz and 3 Hz. These values were chosen based on the perturbation profiles implemented in the experiments conducted in the CAREN (see Section 2.3). We then performed the optimization routine in Section 2.1 and obtained the FSR limits for each amplitude and frequency and for each perturbation modality (six cases for each modality), as well as for the unperturbed walking condition. We modeled the FSR limits for backward and forward loss of balance as second-order polynomials:

$$\dot{x}_n = a_1.x_n^2 + a_2.x_n + a_3 \quad (3)$$

where $\dot{x}_n$ and x_n are the normalized relative velocity and position of the COM, respectively. A second order polynomial was used to model the FSR limits due to our observations from the FSR curvatures and curve fitting errors. Subsequently, we modeled the parameters of these polynomials (a_i) as a function of perturbation amplitude (A) and frequency (f) using a least-square error minimization approach:

$$a_i = b_{1i}.f + b_{2i}.A + b_{3i}.f.A + b_{4i} \quad (i = 1,2,3) \quad (4)$$

2.3. Experimental validation

To evaluate the obtained FSR limits through simulations in Sections 2.1 and 2.2, we compared them with those previously presented in the literature. In addition, experimental data for the cases of perturbed and unperturbed walking were collected. Experiments were conducted using a CAREN (Fig. 3). Fifteen non-disabled individuals having average body height and body mass of 1.79 ± 0.09 m and 78.7 ± 5.8 kg, respectively, and three individuals with amputation (one with unilateral trans-femoral, one with unilateral trans-tibial, and one with unilateral upper limb amputation and sustained traumatic brain injury) (body height: 1.78 ± 0.1 m; body mass: 75.7 ± 3.8 kg) participated in this study. The experimental protocol was approved by the local research ethics board (protocol number: Pro00066076), and all participants gave informed consent. Each participant performed a walking trial including four sessions: One session of 30 m of unperturbed walking, followed by three sessions of 60 m of perturbed walking. Walking trials were performed on a platform-mounted treadmill, which adapted to the speed of walking of each individual to model their natural walking situation. Platform perturbations were in the form of vertical or horizontal displacement, sagittal rotation, or a combination of them, and were initiated after the toe-off instances. Perturbations reached to a maximum amplitude during each trial which increased from low-perturbation trials to high-perturbation ones (amplitude ranging from 1 cm to 6 cm in the vertical and horizontal directions and 0.6° to 3° in rotation) and had a dominant frequency of 1 Hz or 3 Hz. The COM position and velocity, as well as the BOS position and velocity, were calculated using data from the motion capture system (Vicon, UK). The BOS motion was tracked using four markers placed on a rigid plate attached to each foot, and the heel's and toes' position was obtained as a function of these markers' trajectory and based on a calibration procedure before motion recording. The COM motion was tracked using four markers placed on a rigid plate over the sacrum, and based on the location of the COM relative to the

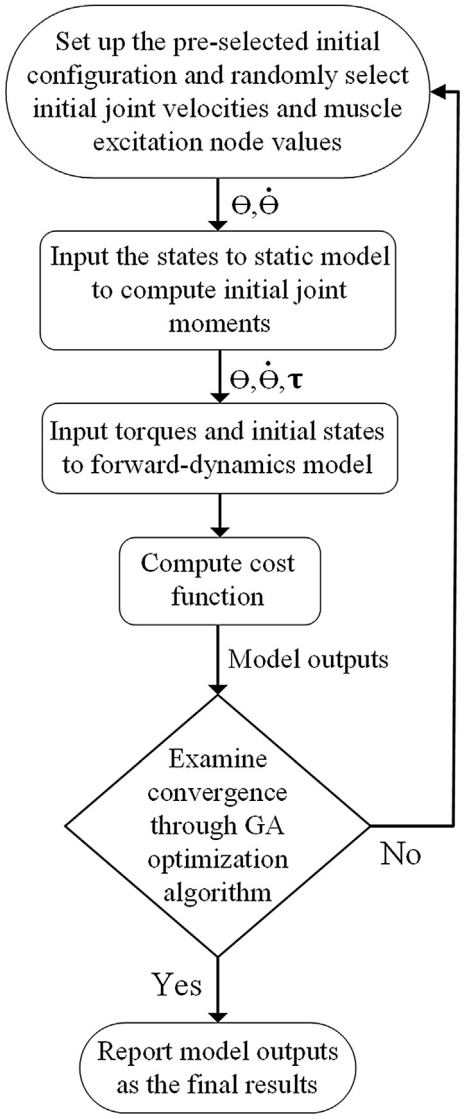

Fig. 2. Flowchart of simulation and optimization process: An initial model was used to determine the initial joint moments at the instance of foot toe-off. Inputs to this model were each joint's initial angle obtained from experimental data. Then, a forward dynamics model was used to perform movement simulation. Inputs to this model were each joint's initial angle, angular velocity, torque, and muscle excitation history.

sacrum reported in the literature (Yang and Pai, 2015). Four additional markers were used to track the motion of the platform. We obtained the COM motion states (with respect to the BOS) and investigated if they were within the FSR obtained through simulations.

3. Result

The FSR limit for backward loss of balance obtained in the present study for non-slip, unperturbed walking was more conservative than that reported by Pai and Patton (1997) who used a two-segment model. Our obtained limit for forward loss of balance was close to what they reported. Our obtained limit for backward loss of balance was, however, less conservative than that obtained by Yang et al. (2007). They used the same body model, but implemented a different optimization cost function and also simulated a slip condition (Fig. 4).

An increase in both the amplitude and frequency of the vertical and horizontal displacements and sagittal rotation resulted in a reduced range of FSR for both backward and forward loss of balance (Fig. 5). Table 1 presents the limits of backward and forward loss of balance, modeled as second-order polynomials for different amplitudes and frequencies of the vertical and horizontal displacements and sagittal rotation of the BOS. The limit of forward loss of balance could be modeled as a line since the coefficients of the second-order term were close to zero.

For each walking perturbation condition, a majority of the experimentally obtained COM motion states of non-disabled individuals and individuals with amputation were within the FSR obtained through simulation (Fig. 6). In trials with the higher perturbation level, we observed more scattered COM motion states at the toe-off instance.

For non-disabled participants, an average of 89.5% of experimentally recorded COM motion states at the toe-off instance were inside the FSR limits for both vertical and horizontal displacement and sagittal rotation conditions (120 to 200 steps) under the low perturbation condition (frequency of 1 Hz and amplitudes of 1 cm and 0.6°). For the high perturbation condition (frequency of 3 Hz and amplitudes of 6 cm and 3°), the mentioned ratio was 70.9%. For participants with amputation, these ratios were 82.4% and 68.2% for low perturbation and high perturbation conditions, respectively. The FSR limits for high and low perturbation conditions were obtained using the coefficients presented in Table 2. Reported values contain both right and left toe-off instances of each participant during perturbed treadmill walking trials. The number of steps varied among participants due to the fact that the walking trials were designed for a fixed walking distance, rather than a fixed number of steps as well the loss of camera recordings for a number of gait cycles.

4. Discussion

The human body faces a variety of walking perturbation modalities during daily life. To reduce the risk of falling due to real-world perturbations, rehabilitation training programs in virtual reality interactive environments such as the CAREN have been developed. Similar to real-world perturbations, these environments can apply walking perturbations using complex motions of a moving platform. The development of individual-specific, efficient rehabilitation programs requires to quantify the dynamic stability during perturbed walking, as a function of the perturbation profile. Although the FSR for unperturbed walking and slip condition have been reported in the literature (Yang et al., 2008; Yang et al., 2011), there is currently no model for the FSR during complex walking perturbations similar to those applied by the CAREN platform. We hypothesized that the complex translational and rotational motions of the CAREN platform can be molded as a series of sinusoidal motions in each direction. The original contribution of this study was to determine the FSR limits as a function of the amplitude and frequency of the sinusoidal movements of BOS in the vertical and horizontal directions and as sagittal rotation. We used a seven-link model of the body previously developed in the literature (Yang et al., 2008). However, we modified the previously suggested dynamic optimization and added additional terms to its cost function to ensure smooth and realistic motion of the body during the swing phase, improved the accuracy of the estimated FSR, and enabled modeling of loss of balance during perturbed walking. The FSR from our simulation process for unperturbed walking derived from our proposed optimization cost function and seven-link model was similar to those previously reported by Pai and Patton (1997) and Yang et al. (2008). Particularly, our study presents a more conservative FSR limit for backward loss of balance compared to (Yang et al., 2008), with the same seven-segment model and a similar optimization cost function. Compar-

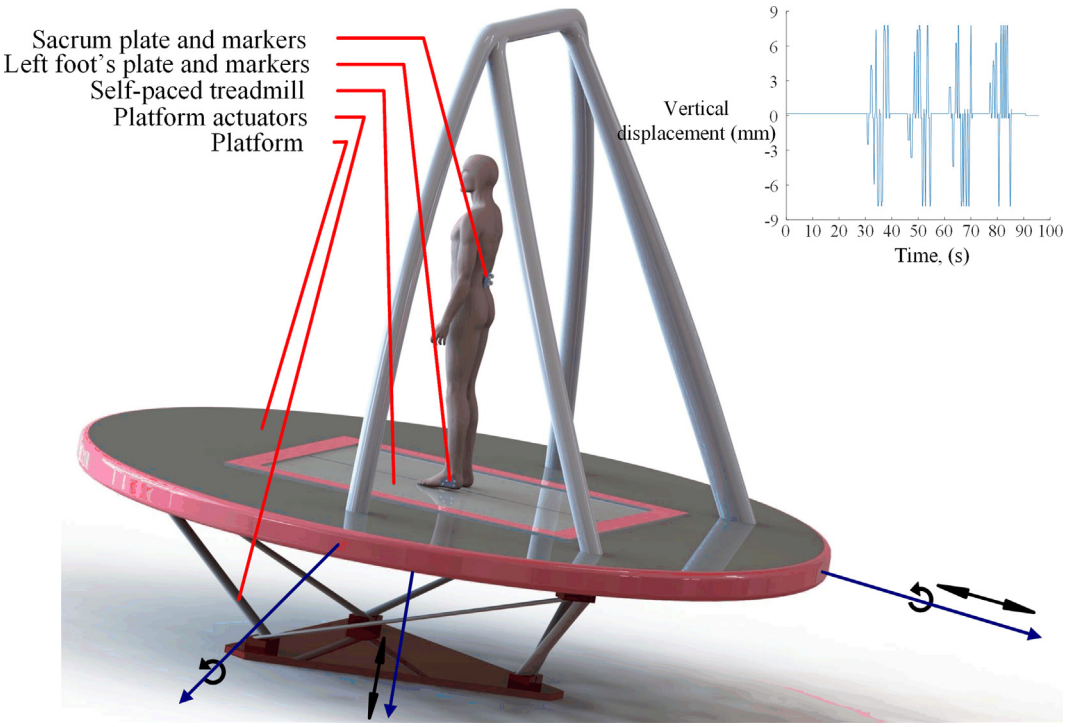

Fig. 3. Illustration of the experimental setup and the CAREN platform. A force plate-embedded split treadmill is installed on a Stewart platform that can apply 3D translational perturbation and rotation perturbation in the sagittal and frontal plane. Perturbations were imposed right after each toe-off and only on the foot in contact with the platform. The toe-off instances were detected in real-time using a motion capture system. The order of perturbation profiles was randomized but the dominant frequencies and amplitudes remained the same across different participants. Platform motions were induced using a series of hydraulic actuators and the axes of rotation of the platform passed through its centre as shown on the figure. A sample perturbation profile for vertical displacement during low perturbation trials is shown on the top-right.

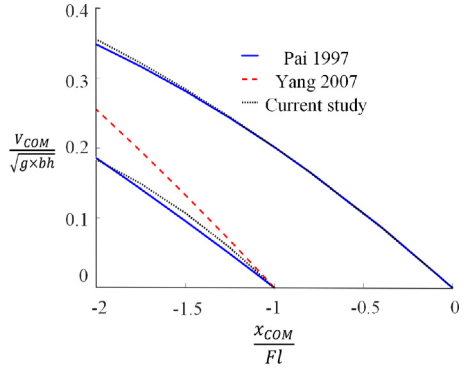

Fig. 4. Limits of the feasible stability range (FSR), obtained for backward and forward loss of balance, in the center of mass (COM) motion state space. COM position and velocity (relative to the base of support; BOS) were normalized to foot length (Fl) and $\sqrt{g \times bh}$ (g: gravitational acceleration; bh: body height), respectively. Values of 0 and −1 on the horizontal axis indicate the COM being located perfectly above the right toe and heel, respectively. These limits (shown as red lines) are compared to those obtained by Pai and Patton (1997) and Yang et al. (2007) for non-slip conditions that used a different number of segments and/or optimization cost function. (For interpretation of the references to colour in this figure legend, the reader is referred to the web version of this article.)

ing the experimentally recorded COM motion states with the modeled limits of FSR can provide mechanistic insights into the human motor control system under perturbed conditions for individuals with different neuromuscular impairments.

We modeled the upper and lower limits of the FSR as second-order polynomials and obtained the polynomial parameters as a function of the amplitude and frequency of for the three BOS motion modalities in the sagittal plane. Our results show that an increase in both amplitude and frequency shrinks the FSR boundaries. This suggests that more conservative strategies are required for balance control of COM motion states in the case of perturbed walking. The practical impact of this study is that our obtained FSR limits (Tables 1 and 2) can be used to calculate FSR limits for other complex BOS perturbations in the sagittal plane with no more need of running the simulations.

The collected COM motion sates were experimentally collected for non-disabled individuals as well as for individuals with trans-femoral or trans-tibial amputation or brain injury during walking, with high and low levels of perturbation. A majority of the COM motion states at the beginning of the swing phase (toe-off instance) were located within the FSR limits. A number of the COM motion states at this instance were outside of the FSR range, with no fall occurring. The portion of the COM motion states lying outside the FSR limits increased from 10.5 to 28.6% (for non-disabled individuals) when increasing the perturbation intensity, which is consistent with the increased variability of gait (Dingwell et al., 1999) expected with higher levels of perturbation.

Note that the presented FSR limits for backward and forward loss of balance are relative measures and do not deterministically predict the loss of balance and falling. Therefore, similar to previous studies, we expect to observe a number of COM motion states outside the estimated FSR, without an incidence of falling (Yang et al., 2008) for the following reasons: First, our proposed model predicted only biomechanical mechanisms of loss of balance. The thresholds for loss of balance and falling may change due to psychological or cognitive reasons. Second, our estimation of the physiological ranges of joint moments and the ability of an individual to control them was based on models reported in the literature (See Supplementary material) (Pandy and Andriacchi, 2010; Zajac, 1989). The model parameters are expected to change as a function

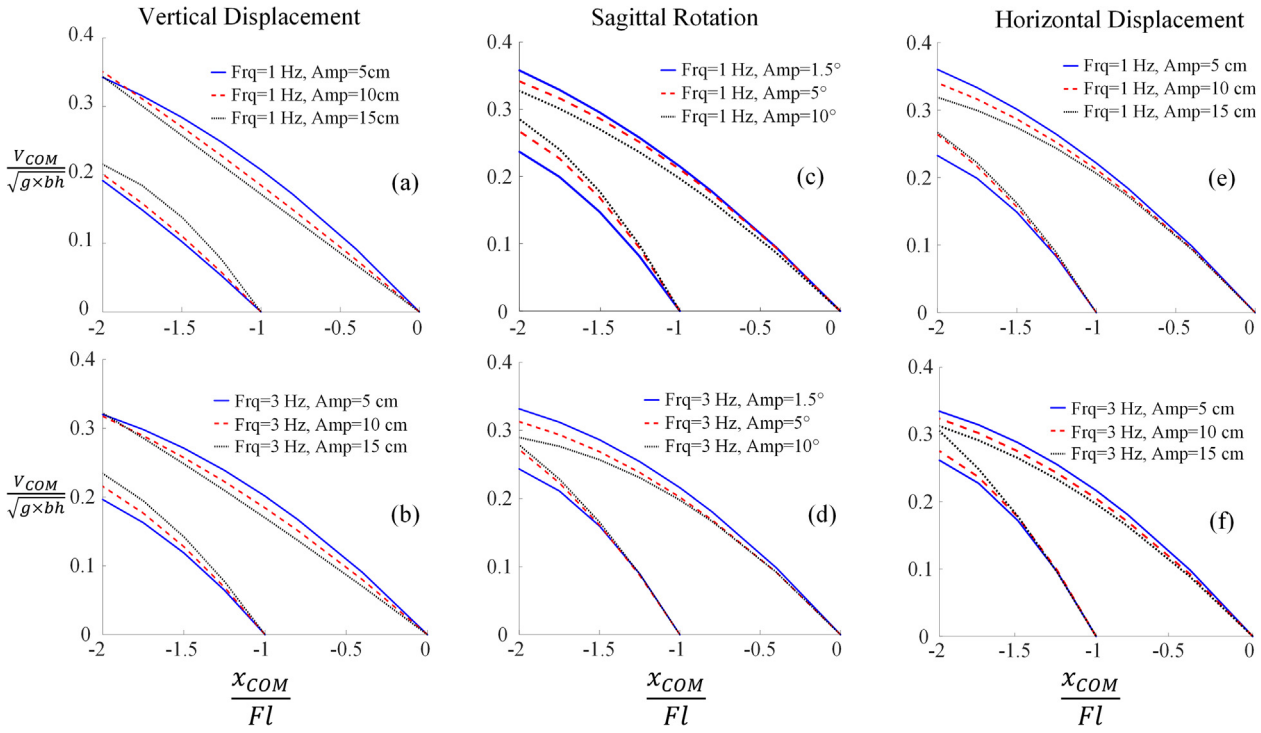

Fig. 5. Effects of frequency and amplitude of the perturbations on the limits of the feasible stability range (FSR). Plots (a–b), (c–d), and (e–f) show the FSR limits when base of support (BOS) perturbations are modeled as sinusoidal movements in the vertical direction, a sinusoidal rotation between foot and the horizontal plane, and sinusoidal movements in the horizontal (anterior-posterior) direction, respectively. The center of mass (COM) position and velocity are normalized as in Fig. 4.

Table 1
Limits of backward and forward loss of balance during walking with vertical and horizontal (anterior-posterior) displacement, and sagittal rotation perturbations of the base of support (BOS). Each type of perturbation is modeled as a sinusoidal motion with different levels of frequency (f) and amplitude (A). For each perturbation condition, the first and second rows indicate a polynomial equation that models the limits of backward and forward loss of balance, respectively. These equations are expressed in the form of $\dot{x}_n = a_1.x_n^2 + a_2.x_n + a_3$, $\dot{x}_n$. x_n stand for COM velocity and position, with respect to the BOS, and normalized to $\sqrt{g \times bh}$ (g: gravitational acceleration; bh: body height) and foot length, respectively. The number in brackets next to each equation indicates the residual value ($\sqrt{\sum (\dot{x}_{n,approximation} - \dot{x}_{n,simulation})^2 / N}$) corresponding to each polynomial's equation. $\dot{x}_{n,approximation}$ is the approximated value of $\dot{x}_n$ obtained through the polynomial equations, $\dot{x}_{n,simulation}$ is the value of $\dot{x}_n$obtained from simulation results and N is the number of samples.

	Limit of backward loss of balance	Limit of forward loss of balance
Vertical displacement		
f = 1 Hz & A = 5 cm	$\dot{x}_n = -0.026x_n^2 - 0.274x_n - 0.244(0.0037)$	$\dot{x}_n = -0.036x_n^2 - 0.243x_n(0.0042)$
f = 1 Hz & A = 10 cm	$\dot{x}_n = -0.041x_n^2 - 0.324x_n - 0.283(0.0070)$	$\dot{x}_n = -0.009x_n^2 - 0.194x_n(0.0012)$
f = 1 Hz & A = 15 cm	$\dot{x}_n = -0.122x_n^2 - 0.582x_n - 0.459(0.0024)$	$\dot{x}_n = -0.001x_n^2 - 0.172x_n(0.0045)$
f = 3 Hz & A = 5 cm	$\dot{x}_n = -0.082x_n^2 - 0.443x_n - 0.361(0.0060)$	$\dot{x}_n = -0.041x_n^2 - 0.243x_n(0.0028)$
f = 3 Hz & A = 10 cm	$\dot{x}_n = -0.080x_n^2 - 0.457x_n - 0.376(0.0037)$	$\dot{x}_n = -0.026x_n^2 - 0.210x_n(0.0036)$
f = 3 Hz & A = 15 cm	$\dot{x}_n = -0.101x_n^2 - 0.536x_n - 0.436(0.0012)$	$\dot{x}_n = -0.009x_n^2 - 0.179x_n(0.0043)$
Sagittal rotation		
f = 1 Hz & A = 1.5°	$\dot{x}_n = -0.129x_n^2 - 0.621x_n - 0.491(0.0055)$	$\dot{x}_n = -0.041x_n^2 - 0.263x_n(0.0045)$
f = 1 Hz & A = 5°	$\dot{x}_n = -0.098x_n^2 - 0.558x_n - 0.460(0.0047)$	$\dot{x}_n = -0.042x_n^2 - 0.254x_n(0.0032)$
f = 1 Hz & A = 10°	$\dot{x}_n = -0.114x_n^2 - 0.610x_n - 0.496(0.0050)$	$\dot{x}_n = -0.047x_n^2 - 0.253x_n(0.0036)$
f = 3 Hz & A = 1.5°	$\dot{x}_n = -0.152x_n^2 - 0.670x_n - 0.548(0.0212)$	$\dot{x}_n = -0.050x_n^2 - 0.266x_n(0.0043)$
f = 3 Hz & A = 5°	$\dot{x}_n = -0.101x_n^2 - 0.574x_n - 0.473(0.0044)$	$\dot{x}_n = -0.045x_n^2 - 0.247x_n(0.0051)$
f = 3 Hz & A = 10°	$\dot{x}_n = -0.104x_n^2 - 0.591x_n - 0.487(0.0049)$	$\dot{x}_n = -0.053x_n^2 - 0.251x_n(0.0038)$
Horizontal displacement		
f = 1 Hz & A = 5 cm	$\dot{x}_n = -0.116x_n^2 - 0.584x_n - 0.468(0.0014)$	$\dot{x}_n = -0.035x_n^2 - 0.251x_n(0.0019)$
f = 1 Hz & A = 10 cm	$\dot{x}_n = -0.140x_n^2 - 0.688x_n - 0.548(0.0038)$	$\dot{x}_n = -0.040x_n^2 - 0.251x_n(0.0029)$
f = 1 Hz & A = 15 cm	$\dot{x}_n = -0.141x_n^2 - 0.707x_n - 0.567(0.0038)$	$\dot{x}_n = -0.033x_n^2 - 0.230x_n(0.0032)$
f = 3 Hz & A = 5 cm	$\dot{x}_n = -0.166x_n^2 - 0.760x_n - 0.594(0.0208)$	$\dot{x}_n = -0.050x_n^2 - 0.266x_n(0.0018)$
f = 3 Hz & A = 10 cm	$\dot{x}_n = -0.164x_n^2 - 0.777x_n - 0.613(0.0033)$	$\dot{x}_n = -0.043x_n^2 - 0.248x_n(0.0028)$
f = 3 Hz & A = 15 cm	$\dot{x}_n = -0.104x_n^2 - 0.620x_n - 0.516(0.0060)$	$\dot{x}_n = -0.041x_n^2 - 0.234x_n(0.0031)$

of an individual's neuromuscular condition, and not considering such variability in our study is a limitation. Third, loss of balance does not usually result in falling but requires an action for recovery. An individual who is at high risk of loss of balance usually adopts a modified control strategy to maintain their balance, such as taking recovery steps or changing the step length during walking. Fourth, assuming the HAT as a rigid segment neglects the motion of the upper limbs and their potential contribution to

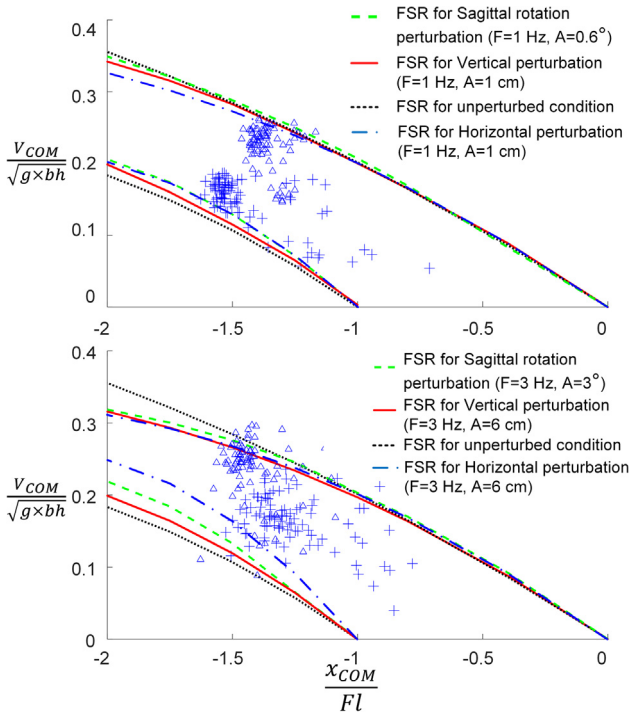

Fig. 6. COM position and velocity obtained experimentally for two walking trials of one representative non-disabled participant (+points) and one case of participant (Δ points) with amputation (feasible stability limits, FSR, obtained through simulation results). + and Δ points illustrate right foot toe-off instances. The top graph is representative of the walking trial with low perturbation intensity (vertical and horizontal displacements, and sagittal rotations with frequency of 1 Hz and amplitudes of 1 cm and 0.6°, respectively). The bottom graph is representative of the walking trial with high perturbation intensity (vertical and horizontal displacements, and sagittal rotations with frequency of 3 Hz and amplitudes of 6 cm and 3°, respectively).

Table 2
The parameters of the polynomial equations that modeled the limits of backward and forward loss of balance in Table 1, modeled as a function of frequency and amplitude of perturbation. This equation is expressed as $\dot{x}_n = a_1.x_n^2 + a_2.x_n + a_3$ for each perturbation condition. Each parameter (a_i: a_1, a_2, or a_3) is modeled as $a_i = b_{1i}.f + b_{2i}.A + b_{3i}f.A + b_{4i}$, where f stands for frequency in Hz and A stands for amplitude in meters (vertical and horizontal displacement perturbation) and radians (sagittal rotation perturbation). The number in brackets next to each equation indicates the residual value ($\sqrt{\sum (a_{i,approximation} - a_{i,interpolation})^2/N}$) corresponding to each coefficient's equation. $a_{i,approximation}$ ($i = 1, 2, 3$) is the approximated value of $a_i$obtained using a least-square error minimization procedure, $a_{i,interpolation}$ is the value of $a_i$reported in the equations in Table 1, and N is the number of samples.

Vertical displacement	
a_1 **for upper limit**	$-0.012f + 0.210A + 0.050f.A - 0.027(0.0019)$
a_2 **for upper limit**	$-0.017f + 0.388A + 0.108f.A - 0.232(0.0034)$
a_3 **for upper limit**	0
a_1 **for lower limit**	$-0.001f - 0.285A - 0.039f.A - 0.040(0.0098)$
a_2 **for lower limit**	$-0.003f - 0.998A - 0.188f.A - 0.304(0.0295)$
a_3 **for lower limit**	$-0.001f - 0.705A - 0.158f.A - 0.263(0.0199)$
Sagittal rotation	
a_1 **for upper limit**	$-0.007f - 0.116A + 0.035f.A - 0.027(0.0012)$
a_2 **for upper limit**	$-0.012f - 0.158A + 0.097f.A - 0.235(0.0033)$
a_3 **for upper limit**	0
a_1 **for lower limit**	$-0.027f - 0.289A + 0.213f.A - 0.073(0.0064)$
a_2 **for lower limit**	$-0.090f - 1.320A + 0.676f.A - 0.419(0.0188)$
a_3 **for lower limit**	$-0.073f - 1.050A + 0.526f.A - 0.342(0.0130)$
Horizontal displacement	
a_1 **for upper limit**	$-0.010f - 0.064A + 0.055f.A - 0.025(0.0010)$
a_2 **for upper limit**	$-0.019f - 0.079A + 0.150f.A - 0.230(0.0024)$
a_3 **for upper limit**	0
a_1 **for lower limit**	$-0.049f - 0.660A + 0.430f.A - 0.061(0.0043)$
a_2 **for lower limit**	$-0.164f - 2.610A + 1.341f.A - 0.368(0.0132)$
a_3 **for lower limit**	$-0.116f - 1.957A + 0.918f.A - 0.307(0.0089)$

walking stability. Although this contribution is reported to be non-significant for slip condition (Marigold, 2002), it is possible that during applied perturbation in our experiments, the COM motion states moved out of the FSR, but that the upper limbs and trunk motion brought the COM motion states back to the FSR. Fifth, we modeled body movements only in the sagittal plane, whereas perturbations and movements in the frontal plane can alter the limits of FSR. These two latter topics should be investigated in the future. Despite these limitations and the influence of these balance mechanisms that must be studied in the future, the present study accomplishes the first step for such future studies. Our study also quantified the challenges that individuals with neuromuscular impairment would face in the presence of BOS perturbation in the sagittal plane and, thus, could provide an assessment to contribute to the development of rehabilitative programs in the future.

5. Conclusions

This study quantified the effect of walking perturbations in the forms of vertical and horizontal displacements of the base of support (ground) and its rotation in the sagittal plane on the FSR against backward and forward loss of balance. Considering the limitations of this study, we can support the integrity of our results by relying on the comparison with FSR limits presented in the literature and on our experimental results from non-disabled individuals and individuals with amputation during walking. The FSR limits provided in this study can be used as a basis for developing rehabilitative programs conducted in virtual reality environments such as the CAREN and for providing training guidelines for patients with walking disabilities. The findings of this study can also enhance our mechanistic understanding of human motor control under different walking perturbation conditions.

Declaration of Competing Interest

None.

Acknowledgments

The authors would like to thank the Department of Research and Technology Development of the Glenrose Rehabilitation Hospital for providing access to the research facility, and especially Dr. Juan Forero, and Mr. Darrell Goertzen and Jeremy Hall for their technical assistance. This work was financially supported by the Natural Sciences and Engineering Research Council of Canada (grant: RGPIN-2016-04106) and the University of Alberta.

Appendix A. Supplementary material

Human body model during dynamic walking. Supplementary data to this article can be found online at https://doi.org/10.1016/j.jbiomech.2019.109315.

References

Anderson, F.C., Pandy, M.G., 2001. Dynamic optimization of human walking. J. Biomech. Eng. 123, 381.
Bruijn, S.M., Meijer, O.G., Beek, P.J., Van Dieen, J.H., 2013. Assessing the stability of human locomotion: a review of current measures. J. R. Soc. Interface 10. 20120999-20120999.
Delp, S.L., Anderson, F.C., Arnold, A.S., Loan, P., Habib, A., John, C.T., Guendelman, E., Thelen, D.G., 2007. OpenSim: open-source software to create and analyze dynamic simulations of movement. IEEE Trans. Biomed. Eng. 54, 1940–1950.
Dingwell, J.B., Ulbrecht, J.S., Boch, J., Becker, M.B., O'Gorman, J.T., Cavanagh, P.R., 1999. Neuropathic gait shows only trends towards increased variability of sagittal plane kinematics during treadmill locomotion. Gait Posture 10, 21–29.
Goswami, A., Thuilot, B., Espiau, B., 2006. Compass-like biped robot Part I: stability and bifurcation of passive gaits. RR-2996, INRIA.

Hausdorff, J.M., Rios, D.A., Edelberg, H.K., 2001. Gait variability and fall risk in community-living older adults: A 1-year prospective study. Arch. Phys. Med. Rehabil. 82, 1050–1056.
Hof, A.L., 2008. The "extrapolated center of mass" concept suggests a simple control of balance in walking. Hum. Mov. Sci. 27, 112–125.
Hof, A.L., Gazendam, M.G.J., Sinke, W.E., 2005. The condition for dynamic stability. J. Biomech. 38, 1–8.
Hurmuzlu, Y., 1993. Dynamics of bipedal gait: Part II—stability analysis of a planar five-link biped. J. Appl. Mech. 60, 337–343.
Kuo, A.D., Donelan, J.M., Ruina, A., 2005. Energetic consequences of walkin Like an inverted pendulum: step to step transitions. Exerc. Sport. Sci. Rev. 33, 88–97.
Madehkhaksar, F., Klenk, J., Sczuka, K., Gordt, K., Melzer, I., Schwenk, M., 2018. The effects of unexpected mechanical perturbations during treadmill walking on spatiotemporal gait parameters, and the dynamic stability measures by which to quantify postural response. PLoS One 13, 1–15.
Marigold, D.S., 2002. Role of the unperturbed limb and arms in the reactive recovery response to an unexpected slip during locomotion. J. Neurophysiol. 89, 1727–1737.
McAndrew, P.M., Wilken, J.M., Dingwell, J.B., 2011. Dynamic stability of human walking in visually and mechanically destabilizing environments. J. Biomech. 44, 644–649.
Pai, Y.C., 2003. Movement termination and stability in standing. Exerc. Sport Sci. Rev. 31, 19–25.
Pai, Y.C., Maki, B.E., Iqbal, K., McIlroy, W.E., Perry, S.D., 2000. Thresholds for step initiation induced by support-surface translation: A dynamic center-of-mass model provides much better prediction than a static model. J. Biomech. 33, 387–392.
Pai, Y.C., Patton, J., 1997. Center of mass velocity-position predictions for balance control [published erratum appears in J Biomech 1998 Feb; 31(2):199]. J Biomech 30, 347–354.
Pai, Y.C., Rogers, M.W., Patton, J., Cain, T.D., Hanke, T.A., 1998. Static versus dynamic predictions of protective stepping following waist-pull perturbations in young and older adults. J. Biomech. 31, 1111–1118.
Pandy, M.G., Andriacchi, T.P., 2010. Muscle and joint function in human locomotion. Annu. Rev. Biomed. Eng.
Robinovitch, S.N., Feldman, F., Yang, Y., Schonnop, R., Leung, P.M., Sarraf, T., Sims-Gould, J., Loughi, M., 2013. Video capture of the circumstances of falls in elderly people residing in long-term care: an observational study. Lancet 381, 47–54.
Stevens, J.A., Sogolow, E.D., 2005. Gender differences for non-fatal unintentional fall related injuries among older adults. Inj. Prev. 11, 115–119.
Winter, D.A., 2005. Biomechanics and Motor Control of Human Movement. John Wiley & Sons, Hoboken, N.J..
Wolf, A., Swift, J.B., Swinney, H.L., Vastano, J.A., 1985. Determining Lyapunov exponents from a time series. Physics 16D (16), 285–317.
Yang, F., Anderson, F.C., Pai, Y.C., 2007. Predicted threshold against backward balance loss in gait. J. Biomech. 40, 804–811.
Yang, F., Anderson, F.C., Pai, Y.C., 2008. Predicted threshold against backward balance loss following a slip in gait. J. Biomech. 41, 1823–1831.
Yang, F., Bhatt, T., Pai, Y.C., 2011. Limits of recovery against slip-induced falls while walking. J. Biomech. 44, 2607–2613.
Yang, F., Espy, D., Pai, Y.C., 2009. Feasible stability region in the frontal plane during human gait. Ann. Biomed. Eng. 37, 2606–2614.
Yang, F., Pai, Y.C., 2015. Can sacral markers approximate center of mass during gait and slip-fall recovery among community-dwelling older adults? J. Biomech. 47, 3807–3812.
Zajac, F.E., 1989. Muscle and tendon: properties, models, scaling, and application to biomechanics and motor control. Crit. Rev. Biomed. Eng.